ACADEMIC PRESS

Available online at www.sciencedirect.com

SCIENCE DIRECT®

Journal of Sound and Vibration 263 (2003) 871–891

JOURNAL OF SOUND AND VIBRATION

www.elsevier.com/locate/jsvi

Piezoelastic vibrations of composite Reissner–Mindlin-type plates

M. Krommer*

Division of Technical Mechanics, Johannes Kepler University of Linz, Altenbergerstr. 69, A-4040 Linz, Austria

Received 18 March 2002; accepted 29 May 2002

Abstract

Linear vibrations of Reissner–Mindlin-type composite plates in the presence of piezoelectric eigenstrains are studied. Piezoelectric eigenstrains are produced by applying electrical loads to piezoelectric layers embedded in or attached to substrate layers. The influence of the mechanical field upon the electric field is taken into account in the modelling, ending up with electro-mechanically coupled field equations and boundary conditions, which describe the mechanical and the electrical dynamic response of the plate.

The mechanical displacements are approximated by means of the kinematic hypothesis of Hencky. The electric potential distribution is assumed to be composed of a superposition of a linear and a parabolic distribution in the thickness direction. The linear part accounts for the electric potential difference between the electrodes of the totally electroded piezoelectric layers. The parabolic part is considered in order to take into account the influence of the mechanical field upon the electric potential by means of the direct piezoelectric effect. A weak two-dimensional formulation of the three-dimensional field equations is obtained by utilizing mechanical and electrical variational principles. This formulation is characterized by resultants of stress and electric displacement. The electro-mechanically coupled behaviour comes into play by means of the constitutive relations. In case the electric potential difference is not prescribed, it can be calculated from a relation, which connects the total electric charge and the electric potential difference to each other. Because this relation is obtained from the Gauss law of electrostatics, requiring integration with respect to the area of the electrode, non-local constitutive relations for the plate are found. The non-local constitutive relations bring a new aspect into the theory of plates. An analysis for the practically interesting one-dimensional case of composite, piezoelectric plates in cylindrical motion completes the paper.

*Tel.: +43-732-2468-9764; fax: +43-732-2468-9763.

E-mail address: krommer@mechatronik.uni-linz.ac.at (M. Krommer).

0022-460X/03/$ - see front matter
doi:10.1016/S0022-460X(02)01169-0

1. Introduction

Over the last few decades, piezoelastic materials have become prominent in the fields of mechatronics, structronic systems and electro-mechanics, see Tani et al. [1] or Tzou [2]. Piezoelectric solids are utilized to realize distributed actuators and sensors for vibration control of flexible structures, cf., Rao and Sunar [3]. In the high-end technological concept of "intelligent" or "smart" structures, sensors and actuators serve as integrated parts of the structure and are combined with automatic control systems, such that the structure is capable of reacting to external disturbances similar to an intelligent being. Frequently, smart structures are realized by means of thin piezoelastic layers equipped with electrodes mounted at their surfaces. Applying an electric potential difference or an electric charge at the electrodes, an electric field emerges within the piezoelectric layer due to the converse piezoelectric effect, generally resulting in deformation or mechanical stress. The piezoelectric layer thus acts as an actuator, capable of affecting the mechanical behaviour of the structure very quickly. Conversely, a deformation of the structure produces an electric field within the piezoelectric layers. This latter direct piezoelectric effect allows utilizing the layer as a sensor. However, the piezoelectric effects result in a multi-field coupling between mechanical and electrical fields. It is important for practical problems, e.g., in the field of active control of structures, to include electro-mechanical coupling into the modelling in order to obtain an acceptable level of accuracy. In the present paper, piezoelastic vibrations of shear-deformable plates are studied.

The classical plate theory for thin plates was established by Kirchhoff [4] in 1850. However, Kirchhoff's fourth order equations included the well-known boundary condition *paradox*, a contradiction between three natural boundary conditions and the possibility of prescribing only two boundary conditions at a free edge of the plate. This paradox, as well as the development of sandwich structures, led to the formulation of shear deformation theories of sixth order by Reissner [5,6], Hencky [7] and Mindlin [8] around 1950. The theory of piezoelastic plates additionally requires the consideration of the equations governing the quasi-static electric field. Mindlin [9] and Tiersten [10] presented early contributions on the wave motion of single-layered piezoelectric plates. Lee [11], Miu [12] and Tauchert [13] developed plate theories assuming the electric field to be independent from variations of the mechanical field, neglecting the direct piezoelectric effect. Hence different electric conditions, e.g., electroded or non-electroded layers are not suitably reflected in the mechanical modelling. To overcome this problem, more recently electrical equations have been incorporated into thin beam and plate theory by numerous authors, such as Benjeddou et al. [14], Rogacheva [15], Ling-Hui [16] and Krommer [17,18]. Accounts for applying these ideas to moderately thick beams and plates have been given by Krommer and Irschik [19,20]. However, these formulations suffer from the fact that electric boundary conditions at the plate edge cannot be satisfied.

In order to incorporate more accurately the variation of mechanical fields and electric fields, numerous theories have been recently developed. Basically, mechanical and electrical fields are expanded into power series in the thickness direction with terms up to the third order, as in Tiersten [21], Yang and Batra [22] and Yang [23]. A different approach can be found in Fernandes and Pouget [24], accounting for thickness variations by means of harmonic functions. Also, discrete layerwise theories and hybrid or mixed formulations can be widely found in the literature, for example Tzou and Ye [25], Lee and Saravanos [26] and Mitchell and Reddy [27]. These higher

order theories and/or discrete layerwise theories and hybrid formulations are typically combined with finite element formulations. Reviews on modelling of piezoelectric laminates can be found in Saravanos and Heyliger [28] or Gopinathan et al. [29].

The present paper focuses on a consistent modelling approach for the dynamic behaviour of moderately thick composite piezoelastic plates, in which the mechanical and electrical responses are accurately accounted for. In the available literature, linear variations of the electric potential are widely used, as in Suresh et al. [30]. Hence, non-linear variations can only be achieved by introducing discrete mathematical layers inside the physical piezoelastic layer. In this paper, a different approach is considered, in which consistency in context with the first order shear deformation theory is obtained by a second order approximation for the electric potential in the thickness direction. Adjusting the approximation to the electric conditions at the electrodes results in a superposition of a linear variation and a parabolic variation with respect to the thickness of the piezoelastic layer. Furthermore, as a new aspect in the theory of plates, the present formulation results in a non-local formulation of the constitutive relations in order to incorporate the equipotential area condition for electroded layers with an unspecified electric potential difference.

Tensor calculus in a two-dimensional Euclidean space is used in this paper, where tensors are printed bold face. The details for notation are found in Bonet and Wood [31].

2. Modelling

Consider a composite plate as shown in Fig. 1. A single point P on the plate in the reference configuration is characterized by its position vector $\boldsymbol{\xi}$ in a plane reference surface and by the normal distance Z from this surface. The plate is composed of N layers, which are assumed perfectly bonded to each other. Each individual layer may be made of piezoelastic materials; if so,

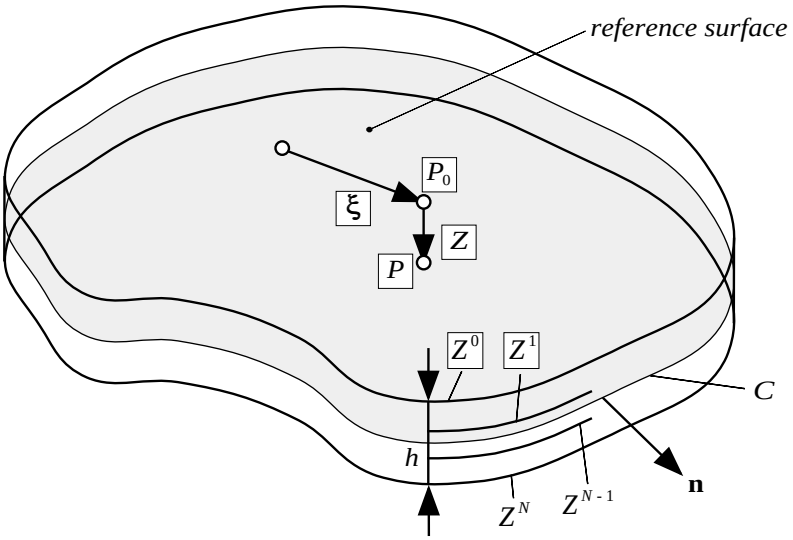

Fig. 1. Geometry of the plate.

electrodes are mounted to its upper and lower surfaces. The moderately large thickness of the plate is h and the kth layer is located between $Z^{k-1} \leqslant Z \leqslant Z^k$. The typical thickness-to-planar dimension ratios (h/L) are within $0.1 \leqslant h/L \leqslant 0.3$. The reference surface is enclosed within the curve C, which has a unit normal vector $\boldsymbol{n}$ pointing outwards.

2.1. Kinematic approximations

The displacement of a point (ξ, Z) is defined by the in-plane displacement vector $\mathbf{u}(\xi, Z)$ and by the out-of-plane deflection $w(\xi, Z)$. The in-plane displacement vector is approximated by means of the Hencky–Mindlin kinematic hypothesis [7,8], and the out-of-plane deflection is considered to be constant with respect to the thickness of the plate

$$\mathbf{u}(\xi, Z) = \mathbf{u}_0(\xi) + Z\boldsymbol{\psi}(\xi), \quad w(\xi, Z) = w_0(\xi). \tag{1}$$

In Eq. (1), $\mathbf{u}_0(\xi)$, $w_0(\xi)$ and $\boldsymbol{\psi}(\xi)$ denote the in-plane displacement vector of points of the reference surface, the out-of-plane deflection of points of the reference surface and the absolute cross-sectional rotation vector, respectively. In a Cartesian co-ordinate system (X, Y), the components of $\boldsymbol{\psi}$ are ψ_x and ψ_y, denoting the rotation of the cross-sections perpendicular to the X- and Y-axis. If the deformation of the plate is considered small, linearized strain can be introduced by means of a plane strain tensor $\boldsymbol{\varepsilon}(\xi, Z)$ and a transverse shear strain vector $\boldsymbol{\gamma}(\xi)$

$$\boldsymbol{\varepsilon}(\xi, Z) = \mathbf{e}(\xi) + Z\boldsymbol{\kappa}(\xi), \quad \boldsymbol{\gamma}(\xi) = \nabla w_0(\xi) + \boldsymbol{\psi}(\xi), \tag{2}$$

where the reference surface strain tensor $\mathbf{e}(\xi)$ and the curvature tensor $\boldsymbol{\kappa}(\xi)$ are defined as

$$\mathbf{e}(\xi) = \tfrac{1}{2}[\nabla \mathbf{u}_0(\xi) + (\nabla \mathbf{u}_0(\xi))^{\mathrm{T}}], \quad \boldsymbol{\kappa}(\xi) = \tfrac{1}{2}[\nabla \boldsymbol{\psi}(\xi) + (\nabla \boldsymbol{\psi}(\xi))^{\mathrm{T}}]. \tag{3}$$

Inside each individual piezoelastic layer, the electric potential $\phi^k(\xi, Z)$ is approximated by the superposition of a linear distribution and a parabolic distribution in the Z direction

$$\phi^k(\xi, Z) = -\frac{V^k}{h^k}(Z - Z^k) + \chi^k(\xi)(Z^2 - Z(Z^{k-1} + Z^k) + Z^{k-1}Z^k). \tag{4}$$

V^k is the electric potential difference in the kth layer, $h^k = Z^{k-1} - Z^k$ denotes the thickness of the kth layer and $\chi^k(\xi)$ is the yet unknown in-plane distribution of the electric potential. This approximation has been used by Krommer and Irschik [32] for beams and by Krommer [33] for plates with piezoelastic layers with prescribed electric potential difference. In the present paper, piezoelastic layers, for which V^k is unknown, are treated in addition. Taking into account the definition of the electric field vector as the negative gradient of the electric potential, the in-plane electric field vector $\mathbf{E}_0^k(\xi, Z)$ and out-of-plane electric field $E_z^k(\xi, Z)$ become

$$\mathbf{E}_0^k(\xi, Z) = -\nabla \phi^k(\xi, Z) = -\nabla \chi^k(\xi)(Z^2 - Z(Z^{k-1} + Z^k) + Z^{k-1}Z^k),$$

$$E_z^k(\xi, Z) = -\frac{\partial \phi^k}{\partial Z}(\xi, Z) = \frac{V^k}{h^k} - 2\chi^k(\xi)(Z - \frac{1}{2}(Z^{k-1} + Z^k)). \tag{5}$$

2.2. Field equations

A generalization of D'Alembert's principle in the formulation of Lagrange for piezoelastic bodies is utilized for a reduction of the three-dimensional problem to a two-dimensional plate

problem

$$\int_{V_0} \boldsymbol{\sigma} : \delta\boldsymbol{\varepsilon}\,\mathrm{d}V + \int_{V_0} \boldsymbol{\tau}\cdot\delta\boldsymbol{\gamma}\,\mathrm{d}V - \sum_{k=1}^{N}\int_{V_0^k} \mathbf{D}_0^k\cdot\delta\mathbf{E}_0^k\,\mathrm{d}V - \sum_{k=1}^{N}\int_{V_0^k} D_z^k\,\delta E_z^k\,\mathrm{d}V$$
$$= -\int_{V_0}\rho_0(\ddot{\mathbf{u}}\cdot\delta\mathbf{u} + \ddot{w}\,\delta w)\,\mathrm{d}V + \int_{S_0}(\mathbf{p}\cdot\delta\mathbf{u} + p_z\,\delta w)\,\mathrm{d}S - \sum_{k=1}^{N}\int_{S_0^k}\tau^{s,k}\,\delta\phi^k\,\mathrm{d}S. \tag{6}$$

This variational principle can be found in Nowacki [34]. The volume and surface of the plate in the reference configuration are V_0 and S_0, whereas V_0^k and S_0^k denote the volume and surface of the kth layer in the reference configuration. The plane stress tensor and transverse shear stress vector are denoted as $\boldsymbol{\sigma}(\boldsymbol{\xi}, Z)$ and $\boldsymbol{\tau}(\boldsymbol{\xi}, Z)$, respectively. $\mathbf{p}$ is a vector with in-plane traction as components and p_z stands for the traction in Z direction. The in-plane electric displacement vector $\mathbf{D}_0^k(\boldsymbol{\xi}, Z)$ and out-of-plane electric displacement $D_z^k(\boldsymbol{\xi}, Z)$ have been introduced in Eq. (6) and $\tau^{s,k}$ denotes the electric charge density at the surface of the kth layer.

Inserting the kinematical approximations of Section 2.1 in the variational principle of Eq. (6) and running through a long but simple derivation, the governing equations of the plate are obtained. These equations characterize the balance of linear momentum and balance of moment of momentum, as well as conservation of electric charge. In the present two-dimensional formulation, the following set of partial differential equations and boundary conditions is obtained:

$$div\,\mathbf{N} + \bar{\mathbf{p}} = P\ddot{\mathbf{u}}_0 + R\ddot{\boldsymbol{\psi}},\quad div\,\mathbf{M} - \mathbf{q} + \bar{\mathbf{p}}_m = R\ddot{\mathbf{u}}_0 + I\ddot{\boldsymbol{\psi}},\quad div\,\mathbf{q} + \bar{p}_z = P\ddot{w}_0,$$
$$\text{at } C:\ [(\mathbf{N}\mathbf{n}) - \bar{\mathbf{n}}]\cdot\delta\mathbf{u}_0 = 0,\quad [(\mathbf{M}\mathbf{n}) - \bar{\mathbf{m}}]\cdot\delta\boldsymbol{\psi} = 0,\quad [(\mathbf{q}\cdot\mathbf{n}) - \bar{q}]\delta w_0 = 0,$$

$$\text{For each piezoelastic layer}:\quad div\,\bar{\bar{\mathbf{D}}}_0^k - \bar{D}_z^k = 0\quad\text{at}\quad C:\bar{\bar{\mathbf{D}}}_0^k\cdot\mathbf{n} = 0. \tag{7}$$

Note that the vertical portions of the piezoelastic layers have been assumed not to be electroded; see Parkus [35] for the resulting boundary condition. In Eq. (7), the resultants of stress, electric displacement and surface traction have been introduced. Thus the in-plane force tensor $\mathbf{N}$, moment tensor $\mathbf{M}$ and transverse shear force vector $\mathbf{q}$ are defined as

$$\mathbf{N} = \sum_{k=1}^{N}\int_{Z^{k-1}}^{Z^k}\boldsymbol{\sigma}\,\mathrm{d}Z,\quad \mathbf{M} = \sum_{k=1}^{N}\int_{Z^{k-1}}^{Z^k}\boldsymbol{\sigma}Z\,\mathrm{d}Z,\quad \mathbf{q} = \sum_{k=1}^{N}\int_{Z^{k-1}}^{Z^k}\boldsymbol{\tau}\,\mathrm{d}Z. \tag{8}$$

Also from Eq. (7), the in-plane electric displacement second moment vector $\bar{\bar{\mathbf{D}}}_0^k$ and out-of-plane electric displacement first moment $\bar{D}_z^k$ in the kth layer are

$$\bar{\bar{\mathbf{D}}}_0^k = \int_{Z^{k-1}}^{Z^k}\mathbf{D}_0^k(Z^2 - Z(Z^{k-1} + Z^k) + Z^{k-1}Z^k)\,\mathrm{d}Z,$$
$$\bar{D}_z^k = -\int_{Z^{k-1}}^{Z^k} 2D_z^k\left(Z - \frac{1}{2}(Z^{k-1} + Z^k)\right)\mathrm{d}Z. \tag{9}$$

The surface traction at the vertical portions of the plate results in an external normal force vector $\bar{\mathbf{n}}$, external moment vector $\bar{\mathbf{m}}$ and external transverse force $\bar{q}$ applied to the plate at the contour C. The surface traction at the upper and lower surface of the plate enters as distributed external in-plane force vector $\bar{\mathbf{p}}$, distributed external moment vector $\bar{\mathbf{p}}_m$ and distributed transverse force $\bar{p}_z$.

Definition of the external loading is

$$\bar{\mathbf{n}} = \sum_{k=1}^{N} \int_{Z^{k-1}}^{Z^k} \mathbf{p}|_C \, \mathrm{d}Z, \quad \bar{\mathbf{m}} = \sum_{k=1}^{N} \int_{Z^{k-1}}^{Z^k} \mathbf{p}|_C Z \, \mathrm{d}Z, \quad \bar{q} = \sum_{k=1}^{N} \int_{Z^{k-1}}^{Z^k} p_z|_C \, \mathrm{d}Z,$$

$$\bar{\mathbf{p}} = \mathbf{p}|_{Z^u} + \mathbf{p}|_{Z^l}, \quad \bar{\mathbf{p}}_m = \mathbf{p}|_{Z^u} Z^u + \mathbf{p}|_{Z^l} Z^l, \quad \bar{p}_z = p_z|_{Z^u} + p_z|_{Z^l}, \tag{10}$$

where Z^u and Z^l denote the distance of the upper surface and the lower surface of the plate from the reference surface, respectively. Finally, linear, coupling and rotatory inertia P, R and I are

$$(P, R, I) = \sum_{k=1}^{N} \int_{Z^{k-1}}^{Z^k} \rho_0^k (1, Z, Z^2) \, \mathrm{d}Z \tag{11}$$

and ρ_0^k is the mass density of the kth layer in the reference configuration.

2.3. Constitutive relations

Materials of symmetry class 2mm are considered with the polarization in the Z direction, see Eringen and Maugin [36]. The stress component σ_{ZZ} is assumed to be negligible. In the small deformation range, the plane stress tensor and transverse shear stress vector in the kth layer can be written as

$$\boldsymbol{\sigma}^k = \mathbf{C}^k : \boldsymbol{\varepsilon} - \bar{\mathbf{e}}^k E_z^k, \quad \boldsymbol{\tau}^k = \mathbf{G}^k \boldsymbol{\gamma} - \bar{\mathbf{h}}^k \mathbf{E}_0^k. \tag{12}$$

Here $\mathbf{C}^k$ is the fourth order tensor of elastic moduli for plane stress and $\mathbf{G}^k$ is the second order tensor of shear moduli. $\bar{\mathbf{e}}^k$ and $\bar{\mathbf{h}}^k$ are the second order tensors of piezoelectric moduli. The electric displacement can be written as

$$\mathbf{D}_0^k = \bar{\mathbf{h}}^k \boldsymbol{\gamma} + \boldsymbol{\epsilon}^k \mathbf{E}_0^k, \quad D_z^k = \bar{\mathbf{e}}^k : \boldsymbol{\varepsilon} + \eta^k E_z^k, \tag{13}$$

where $\boldsymbol{\epsilon}^k$ denotes the second order in-plane permittivity tensor and η^k is the out-of-plane permittivity. Eqs. (12) and (13) are inserted into definitions given by Eqs. (8) and (9), resulting in the following formulation for the in-plane force tensor $\mathbf{N}$, moment tensor $\mathbf{M}$, transverse shear force vector $\mathbf{q}$, in-plane electric displacement second moment vector $\bar{\bar{\mathbf{D}}}_0^k$ and out-of-plane electric displacement first moment $\bar{D}_z^k$:

$$\begin{bmatrix} \mathbf{N} \\ \mathbf{M} \\ \vec{\bar{D}}_z \end{bmatrix} = \begin{bmatrix} \mathbf{A} : & \mathbf{B} : & \vec{\mathbf{0}}^{\mathrm{T}} \\ \mathbf{B} : & \mathbf{D} : & \vec{\bar{\mathbf{e}}}^{\mathrm{T}} \\ \vec{\mathbf{0}} : & \vec{\bar{\mathbf{e}}} : & \bar{\bar{\eta}} \end{bmatrix} \begin{bmatrix} \mathbf{e} \\ \boldsymbol{\kappa} \\ \vec{\chi} \end{bmatrix} - \begin{bmatrix} \mathbf{N}^a \\ \mathbf{M}^a \\ \vec{0} \end{bmatrix} \quad \begin{bmatrix} \mathbf{q} \\ \bar{\bar{\mathbf{D}}}_0 \end{bmatrix} = \begin{bmatrix} \mathbf{S} & \vec{\bar{\mathbf{h}}}^{\mathrm{T}} \\ \vec{\bar{\mathbf{h}}} & \bar{\bar{\boldsymbol{\epsilon}}} \end{bmatrix} \begin{bmatrix} \boldsymbol{\gamma} \\ \nabla \vec{\chi} \end{bmatrix}. \tag{14}$$

In Eq. (14), $\mathbf{A}$, $\mathbf{B}$ and $\mathbf{D}$ are extensional, bending–extension coupling and bending stiffness fourth order tensors and $\mathbf{S}$ is the shear stiffness second order tensor. Definitions are

$$(\mathbf{A}, \mathbf{B}, \mathbf{D}) = \sum_{k=1}^{N} \int_{Z^{k-1}}^{Z^k} \mathbf{C}^k (1, Z, Z^2) \, \mathrm{d}Z, \quad \mathbf{S} = K \sum_{k=1}^{N} \int_{Z^{k-1}}^{Z^k} \mathbf{G}^k \, \mathrm{d}Z, \tag{15}$$

where K is the shear correction coefficient, see Reddy [37]. Column matrices, characterized by an arrow, and square matrices, characterized by a double arrow, have been introduced in Eq. (14).

These matrices have to be distinguished from the tensor notation used throughout this paper; hence they are not written in bold face. They have been introduced only in order to account for each individual piezoelastic layer in a contracted notation. The dimension of these matrices is equal to the number of piezoelectric layers. Components are either scalars, $\vec{\vec{D}}_z$, $\overleftrightarrow{\hat{\eta}}$, $\vec{\chi}$ and $\vec{0}$, vectors, $\vec{\vec{\mathbf{D}}}_0$ and $\nabla\vec{\chi}$, or second order tensors, $\vec{\mathbf{0}}$, $\vec{\hat{\mathbf{e}}}$, $\vec{\hat{\mathbf{h}}}$ and $\overleftrightarrow{\hat{\boldsymbol{\epsilon}}}$. Components of the column matrices $\vec{\hat{\mathbf{e}}}$ and $\vec{\hat{\mathbf{h}}}$ are

$$\hat{\mathbf{e}}^k = 2\int_{Z^{k-1}}^{Z^k} \bar{\mathbf{e}}^k Z\left(Z - \frac{1}{2}(Z^{k-1}+Z^k)\right) \mathrm{d}Z,$$

$$\hat{\mathbf{h}}^k = \int_{Z^{k-1}}^{Z^k} \bar{\mathbf{h}}^k (Z^2 - Z(Z^{k-1}+Z^k) + Z^{k-1}Z^k)\,\mathrm{d}Z \tag{16}$$

and the diagonal matrices $\overleftrightarrow{\hat{\eta}}$ and $\overleftrightarrow{\hat{\boldsymbol{\epsilon}}}$ have the following components:

$$\hat{\eta}^k = -4\int_{Z^{k-1}}^{Z^k} \eta^k \left(Z - \frac{1}{2}(Z^{k-1}+Z^k)\right)^2 \mathrm{d}Z,$$

$$\hat{\boldsymbol{\epsilon}}^k = -\int_{Z^{k-1}}^{Z^k} \boldsymbol{\epsilon}'^k (Z^2 - Z(Z^{k-1}+Z^k) + Z^{k-1}Z^k)^2\,\mathrm{d}Z. \tag{17}$$

Finally, $\mathbf{N}^a$ and $\mathbf{M}^a$ characterize the piezoelectric actuation via the electric potential difference V^k in the piezoelastic layers. Definitions are

$$(\mathbf{N}^a, \mathbf{M}^a) = \sum_{k=1}^{N} \int_{Z^{k-1}}^{Z^k} \bar{\mathbf{e}}^k \frac{V^k}{h^k}(1, Z)\,\mathrm{d}Z. \tag{18}$$

In case the electric potential difference is prescribed for each piezoelastic layer, the electromechanically coupled initial-boundary-value problem, Eqs. (7) and (14), can be solved. However V^k need not be prescribed in every layer, and thus must be pre-calculated.

If V^k is not prescribed in the kth layer, the total electric charge Q^k at one of the two electrodes is prescribed. For example, for electrodes that are left open, the total charge has to be constant with respect to time; hence without any loss of generality, it can be taken as zero. A relation between the potential difference and the total charge is easily found by utilizing the Gauss law of electrostatics

$$Q^k = \oint_{H^k} \mathbf{D}^k \cdot \mathrm{d}\mathbf{H}. \tag{19}$$

Eq. (19) is a three-dimensional formulation, not suitable for the present plate theory. Practically, the surface area integral is reduced to an integral over the area of the electrode, rendering the total charge Q^k at the upper electrode, which is identical to the negative total charge at the lower electrode

$$Q^k = \int_A D_z^k\big|_{Z^{k-1}}\,\mathrm{d}A = \int_A D_z^k\big|_{Z^k}\,\mathrm{d}A. \tag{20}$$

Here, A is the area enclosed by the curve C. Inserting the constitutive relation for D_z^k from Eq. (13), and the constitutive relation for $\bar{D}_z^k$ from Eq. (14), into Eq. (20) and utilizing the conservation of

charge as defined by the last relation of Eq. (7), the following relation is found:

$$y^k = Q^k - C^k V^k = \frac{\eta^k}{h^k} \int_A \left[\int_{Z^{k-1}}^{Z^k} \frac{\bar{\mathbf{e}}^k : \boldsymbol{\varepsilon}}{\eta^k} \mathrm{d}Z \right] \mathrm{d}A. \tag{21}$$

y^k denotes the general sensor signal of the layer and C^k is the capacitance of the layer, $C^k = \eta^k A/h^k$. Taking into account Eq. (21) in the approximation of the electric potential from Eq. (4), a general formulation is found in the form

$$\begin{aligned} \phi^k = & -\left[\frac{V^k}{h^k}(Z - Z^k)\kappa^{V,k} + \frac{Q^k}{\eta^k A}(Z - Z^k)\kappa^{Q,k} \right] \\ & + \left[\frac{1}{A} \int_A \frac{1}{h^k} \int_{Z^{k-1}}^{Z^k} \frac{\bar{\mathbf{e}}^k : \boldsymbol{\varepsilon}}{\eta^k} \mathrm{d}Z \, \mathrm{d}A \right] (Z - Z^k)\kappa^{Q,k} + \chi^k (Z^2 - Z(Z^{k-1} + Z^k) + Z^{k-1} Z^k). \end{aligned} \tag{22}$$

In Eq. (22), tracers $\kappa^{V,k}$ and $\kappa^{Q,k}$ have been introduced in order to characterize piezoelastic layers with either prescribed electric potential difference V^k ($\kappa^{V,k} = 1$) or prescribed total charge Q^k ($\kappa^{Q,k} = 1$). Note that the electric potential distribution in Eq. (22) automatically satisfies the equipotential area condition at the location of the electrodes. In case of prescribed electric charge, this condition can only be satisfied by the present formulation. Eq. (21) additionally is inserted into Eq. (18), replacing V^k by Q^k in case the electric potential difference is not prescribed. After a long but simple reformulation, the final form of the constitutive relations reads

$$\begin{aligned} \begin{bmatrix} \mathbf{N} \\ \mathbf{M} \\ \vec{\vec{D}}_z \end{bmatrix} &= \begin{bmatrix} \mathbf{A}: & \mathbf{B}: & \vec{\mathbf{0}}^{\mathrm{T}} \\ \mathbf{B}: & \mathbf{D}: & \vec{\vec{\mathbf{e}}}^{\mathrm{T}} \\ \vec{\mathbf{0}}: & \vec{\vec{\mathbf{e}}}: & \vec{\vec{\eta}} \end{bmatrix} \begin{bmatrix} \mathbf{e} \\ \boldsymbol{\kappa} \\ \vec{\chi} \end{bmatrix} - \begin{bmatrix} \mathbf{N}^{a,eff} \\ \mathbf{M}^{a,eff} \\ \vec{0} \end{bmatrix} + \begin{bmatrix} \mathbf{a}: & \mathbf{b}: & \vec{\mathbf{0}}^{\mathrm{T}} \\ \mathbf{b}: & \mathbf{d}: & \vec{\mathbf{0}}^{\mathrm{T}} \\ \vec{\mathbf{0}}: & \vec{\mathbf{0}}: & \vec{\vec{0}} \end{bmatrix} \frac{1}{A} \int_A \begin{bmatrix} \mathbf{e} \\ \boldsymbol{\kappa} \\ \vec{\chi} \end{bmatrix} \mathrm{d}A, \\ \begin{bmatrix} \mathbf{q} \\ \vec{\vec{\mathbf{D}}}_0 \end{bmatrix} &= \begin{bmatrix} \mathbf{S} & \vec{\hat{\mathbf{h}}}^{\mathrm{T}} \\ \vec{\hat{\mathbf{h}}} & \vec{\vec{\hat{\boldsymbol{\epsilon}}}} \end{bmatrix} \begin{bmatrix} \boldsymbol{\gamma} \\ \nabla\vec{\chi} \end{bmatrix}. \end{aligned} \tag{23}$$

Comparing Eq. (23) to Eq. (14), it is seen that additional non-local terms have entered the constitutive relations for the in-plane force tensor $\mathbf{N}$ and the moment tensor $\mathbf{M}$. For thin beams and plates, this formulation has been introduced by Krommer [17,18], where a discussion on the necessity of using the non-local formulation for the purpose of satisfying the equipotential area condition is given. The non-local terms relate the average values of the reference surface strain tensor and of the curvature tensor to the in-plane force tensor and the moment tensor via the so-called non-local extensional, bending–extension coupling and bending stiffness fourth order tensors

$$(\mathbf{a}, \mathbf{b}, \mathbf{d}) = \sum_{k=1}^{N} \int_{Z^{k-1}}^{Z^k} \kappa^{Q,k} \frac{\bar{\mathbf{e}}^k \otimes \bar{\mathbf{e}}^k}{\eta^k} \left(1, Z, Z\frac{1}{2}(Z^{k-1} + Z^k)\right) \mathrm{d}Z. \tag{24}$$

Note that the formulation of Eqs. (23) and (24) is valid only if $\bar{\mathbf{e}}^k$ and η^k do not vary with respect to the area of the plate. Finally, the effective piezoelectric actuating in-plane force tensor and moment

tensor, which depend only on either the electric potential difference or total charge, become

$$(\mathbf{N}^{a,eff}, \mathbf{M}^{a,eff}) = \sum_{k=1}^{N} \int_{Z^{k-1}}^{Z^k} \bar{\mathbf{e}}^k \left[\kappa^{V,k} \frac{V^k}{h^k} + \kappa^{Q,k} \frac{Q^k}{\eta^k A} \right] (1, Z)\, \mathrm{d}Z. \tag{25}$$

Eqs. (7) and (23) complete the electro-mechanically coupled initial-boundary-value problem. In the context of linear piezoelectricity, this formulation represents a straightforward extension of the Reissner–Mindlin–plate theory with respect to electro-mechanical coupling.

3. Analysis of plates in cylindrical motion

In this section, symmetrically laminated plates in cylindrical motion are analyzed in detail. Symmetry is assumed with respect to the lamination scheme as well as with respect to the type of electric loading. As a consequence of this symmetry, in-plane motion and out-of-plane motion become de-coupled, $R = 0$, $\mathbf{B} = \mathbf{0}$, $\mathbf{b} = \mathbf{0}$. For the cylindrical motion of a plate panel, the balance laws of Eq. (7) and the constitutive relations of Eq. (23) simplify according to

$$\frac{\partial}{\partial X} n_{xx} + \bar{p}_x = P\ddot{u}_x, \quad \frac{\partial}{\partial X} m_{xx} - q_x + \bar{p}_m = I\ddot{\psi}_x, \quad \frac{\partial}{\partial X} q_x + \bar{p}_z = P\ddot{w}_0,$$

$$\text{at } X = (0, L): \; n_{xx} = \bar{n} \;\text{ or }\; u_x = 0, \quad m_{xx} = \bar{m} \;\text{ or }\; \psi_x = 0, \quad q_x = \bar{q} \;\text{ or }\; w_0 = 0,$$

$$\text{For each piezoelastic layer}: \frac{\partial}{\partial X} \bar{\bar{D}}_x^k - \bar{D}_z^k = 0 \quad \text{at } X = (0, L): \; \bar{\bar{D}}_x^k = 0, \tag{26}$$

$$\begin{bmatrix} n_{xx} \\ m_{xx} \\ \vec{\bar{D}}_z \end{bmatrix} = \begin{bmatrix} A & 0 & \vec{0}^{\mathrm{T}} \\ 0 & D & \vec{\hat{e}}^{\mathrm{T}} \\ \vec{0} & \vec{\hat{e}} & \overleftrightarrow{\hat{\eta}} \end{bmatrix} \begin{bmatrix} e \\ \kappa \\ \vec{\chi} \end{bmatrix} - \begin{bmatrix} n^{a,eff} \\ m^{a,eff} \\ \vec{0} \end{bmatrix} + \begin{bmatrix} a & 0 & \vec{0}^{\mathrm{T}} \\ 0 & d & \vec{0}^{\mathrm{T}} \\ \vec{0} & \vec{0} & \overleftrightarrow{0} \end{bmatrix} \frac{1}{L} \int_0^L \begin{bmatrix} e \\ \kappa \\ \vec{\chi} \end{bmatrix} \mathrm{d}X,$$

$$\begin{bmatrix} q_x \\ \vec{\bar{\bar{D}}}_x \end{bmatrix} = \begin{bmatrix} S & \vec{\hat{h}}^{\mathrm{T}} \\ \vec{\hat{h}} & \overleftrightarrow{\hat{\boldsymbol{\epsilon}}} \end{bmatrix} \begin{bmatrix} \gamma \\ \dfrac{\partial}{\partial X} \vec{\chi} \end{bmatrix}. \tag{27}$$

The cylindrical motion takes place in the (X, Z)-plane. The extension of the panel in X direction is L. In Eq. (27), reference surface strain e, curvature κ and transverse shear strain γ have been introduced and are defined as

$$e = \frac{\partial}{\partial X} u_x, \quad \kappa = \frac{\partial}{\partial X} \psi_x, \quad \gamma = \frac{\partial}{\partial X} w_0 + \psi_x. \tag{28}$$

Extensional, bending and transverse shear stiffness A, D and S, non-local extensional and bending stiffness a and d, piezoelectric parameters $\hat{e}^k$ and $\hat{h}^k$, permittivity parameters $\hat{\eta}^k$ and $\hat{\boldsymbol{\epsilon}}^k$ and

effective piezoelectric actuating in-plane force and moment are

$$(A, D) = \sum_{k=1}^{N} \int_{Z^{k-1}}^{Z^k} Y^k(1, Z^2)\,\mathrm{d}Z, \quad S = K \sum_{k=1}^{N} \int_{Z^{k-1}}^{Z^k} G^k \mathrm{d}Z,$$

$$(a, d) = \sum_{k=1}^{N} \int_{Z^{k-1}}^{Z^k} \kappa^{Q,k} \frac{\bar{e}^k \bar{e}^k}{\eta^k} (1, Z \frac{1}{2}(Z^{k-1} + Z^k))\,\mathrm{d}Z.$$

$$\hat{e}^k = \int_{Z^{k-1}}^{Z^k} 2\bar{e}^k Z(Z - \frac{1}{2}(Z^{k-1} + Z^k))\,\mathrm{d}Z,$$

$$\hat{h}^k = \int_{Z^{k-1}}^{Z^k} \bar{h}^k (Z^2 - Z(Z^{k-1} + Z^k) + Z^{k-1} Z^k)\,\mathrm{d}Z,$$

$$\hat{\eta}^k = -4 \int_{Z^{k-1}}^{Z^k} \eta^k (Z - \frac{1}{2}(Z^{k-1} + Z^k))^2 \mathrm{d}Z,$$

$$\hat{\boldsymbol{\epsilon}}^k = -\int_{Z^{k-1}}^{Z^k} \boldsymbol{\epsilon}^k (Z^2 - Z(Z^{k-1} + Z^k) + Z^{k-1} Z^k)^2\,\mathrm{d}Z. \tag{29}$$

$$(n^{a,eff}, m^{a,eff}) = \sum_{k=1}^{N} \int_{Z^{k-1}}^{Z^k} \bar{e}^k \left[\kappa^{V,k} \frac{V^k}{h^k} + \kappa^{Q,k} \frac{Q^k}{\eta^k L} \right] (1, Z)\,\mathrm{d}Z,$$

The significance of Young's modulus Y^k, shear modulus G^k, piezoelectric coefficients $\bar{e}^k$ and $\bar{h}^k$ and electric permittivities η^k and $\boldsymbol{\epsilon}^k$ is found in the appendix.

The analysis of the initial-boundary-value problem defined by Eqs. (26) and (27) is performed by a transition matrix procedure. The load vector $\vec{\mathbf{f}}(X, t)$ and the state vector $\vec{\mathbf{z}}(X, t)$ are introduced in the form

$$\begin{aligned} \vec{\mathbf{f}}(X, t) &= \vec{\mathbf{f}}(X) \mathrm{e}^{\mathrm{i}\omega t} \\ &= \left[\frac{n^{a,eff}}{A}(X) \quad \frac{m^{a,eff}}{D}(X) \quad 0 \quad \vec{0}^{\mathrm{T}} \quad -\bar{p}_x(X) \quad -\bar{p}_m(X) \quad -\bar{p}_z(X) \quad \frac{\vec{\hat{e}}^{\mathrm{T}} m^{a,eff}}{D}(X) \right]^{\mathrm{T}} \mathrm{e}^{\mathrm{i}\omega t}, \end{aligned}$$

$$\begin{aligned} \vec{\mathbf{z}}(X, t) &= \vec{\mathbf{z}}(X) \mathrm{e}^{\mathrm{i}\omega t} \\ &= \left[u_x(X) \quad \psi_x(X) \quad w_0(X) \quad \vec{\chi}^{\mathrm{T}}(X) \quad n_{xx}(X) \quad m_{xx}(X) \quad q_x(X) \quad \vec{\bar{D}}_x^{\mathrm{T}}(X) \right]^{\mathrm{T}} \mathrm{e}^{\mathrm{i}\omega t}, \end{aligned} \tag{30}$$

where ω denotes the driving frequency of the external loading. The following formulation of the first order system of $(6+2n)$ ordinary differential equations is obtained from Eqs (26) and (27)

$$\frac{\partial}{\partial X} \vec{z}(X) = \vec{\vec{A}}(\omega) \vec{z}(X) + \vec{\vec{a}}(\vec{z}(L) - \vec{z}(0)) + \vec{f}(X), \tag{31}$$

where n is the number of the piezoelastic layers. The non-vanishing components of the system matrices $\vec{\vec{a}}$ and $\vec{\vec{A}}(\omega)$, which are understood as either scalars, column matrices or square

matrices are

$$A_{15}=\frac{1}{A},\quad A_{24}=-\frac{\vec{\hat{e}}^{\mathrm{T}}}{D},\quad A_{26}=\frac{1}{D},\quad A_{32}=-1,\quad A_{37}=\frac{1}{\bar{S}},\quad A_{38}=-\frac{\vec{\hat{h}}^{\mathrm{T}}\overleftrightarrow{\hat{\epsilon}}^{-1}}{\bar{S}},$$

$$A_{47}=-\frac{\overleftrightarrow{\hat{\epsilon}}^{-1}\vec{\hat{h}}}{S},$$

$$A_{48}=\overleftrightarrow{\bar{\epsilon}}^{-1},\quad A_{51}=-P\omega^2,\quad A_{62}=-I\omega^2,\quad A_{67}=1,\quad A_{73}=-P\omega^2,$$

$$A_{84}=\overleftrightarrow{\bar{\eta}},\quad A_{86}=\frac{\vec{\hat{e}}}{D},$$

$$a_{11}=-\frac{1}{L}\frac{a}{A},\quad a_{22}=-\frac{1}{L}\frac{d}{D},\quad a_{82}=-\frac{\vec{\hat{e}}}{L}\frac{d}{D} \tag{32}$$

with the new parameters $\bar{S}=S-\vec{\hat{h}}^{\mathrm{T}}\overleftrightarrow{\hat{\epsilon}}^{-1}\vec{\hat{h}}$, $\overleftrightarrow{\bar{\epsilon}}=\overleftrightarrow{\epsilon}-\vec{\hat{h}}\vec{\hat{h}}^{\mathrm{T}}S^{-1}$ and $\overleftrightarrow{\bar{\eta}}=\overleftrightarrow{\hat{\eta}}-\vec{\hat{e}}\vec{\hat{e}}^{\mathrm{T}}D^{-1}$. Applying the Laplace transformation to Eq. (31), rearranging terms and applying the inverse Laplace transformation yields the following transition matrix formulation:

$$\vec{z}(X)=\overleftrightarrow{U}_0(X,\omega)\vec{z}(0)+\overleftrightarrow{U}_L(X,\omega)\vec{z}(L)+\vec{\bar{f}}(X,\omega). \tag{33}$$

The frequency-dependent transition matrices and load vector are defined as

$$\overleftrightarrow{U}_0(X,\omega)=\overleftrightarrow{A}(X,\omega)*[\overleftrightarrow{I}-\overleftrightarrow{a}],\quad \overleftrightarrow{U}_L(X,\omega)=\overleftrightarrow{A}(X,\omega)*\overleftrightarrow{a},\quad \vec{\bar{f}}(X,\omega)=\overleftrightarrow{A}(X,\omega)*\vec{f}(X), \tag{34}$$

where $*$ denotes the convolution integral and the matrix $\overleftrightarrow{A}(X,\omega)$ is the inverse Laplace transformation of $[s\overleftrightarrow{I}-\overleftrightarrow{A}(\omega)]^{-1}$, with s denoting the parameter of the Laplace transformation. In Eq. (33), the state vector at $X=(0,L)$ is required. For classical homogenous support conditions, one of the components of each of the four conjugate pairs (u_x,n_{xx}), (ψ_x,m_{xx}), (w_0,q_x) and $(\vec{\chi},\vec{\bar{\bar{D}}}_x)$ vanishes. $(6+2n)$ unknowns therefore remain in the state vectors at $X=(0,L)$. These can be easily calculated by evaluating the state vector at $X=L$, which renders $(6+2n)$ equations for the $(6+2n)$ unknowns. The present transition matrix formulation can be advantageously utilized for the analysis of free and forced vibrations.

3.1. Numerical examples

For the numerical analysis, a simple geometry is considered. The extension of the plate panel in X direction is 1 m and the total thickness is 0.1 m. Two identical piezoelastic layers are perfectly bonded to each other, with electrodes at the interface and at the upper and lower sides of the panel. The electrode at the interface is grounded. At the outer electrodes, electrical loading is applied skew-symmetric with respect to the reference surface; hence pure bending of the panel is produced. PZT-5A is used for the piezoelastic layers; the material parameters are given in the appendix. This geometry ensures the symmetry required for the analysis in Section 3. Furthermore, the general formulation of Section 3 is dramatically simplified. It is sufficient to consider only one unknown in-plane distribution of the electric potential χ, because it is identical in the two layers.

3.1.1. Free vibrations

In order to show the capability of the present theory to accurately account for the electro-mechanical coupling present in piezoelastic structures, natural frequencies are calculated for different support conditions. The outer electrodes are either short-circuited, $V^1 = V^2 = 0$, or left open, $Q^1 = Q^2 = 0$. The analytic results are compared to electro-mechanically coupled finite element (FE) calculations, for which the commercially available code Abaqus Version 5.8 is used. In the FE calculations, plane strain elements in the (X, Z)-plane of type CPE4E are utilized. Electrodes that are left open are modelled by stating that the node set, which defines the electrode has to have a space-wise constant electric potential distribution, thus facilitating a comparison to the present non-local theory. Furthermore, purely elastic solutions are also presented, with the purpose of pointing out the influence of electro-mechanical coupling. These solutions neglect the piezoelectric behaviour. A comparison with analytic solutions for plane strain is omitted, because homogenous Dirichlet-type electric boundary conditions are considered in these solutions, see e.g., Heyliger and Brooks [38].

In Table 1, the first six natural frequencies for a hinged–hinged panel are presented. It can be seen that the absolute values for the analytic solution are significantly smaller then the ones calculated by Abaqus. However, this behaviour is reflected by the elastic solution (elastic), by the solution for short-circuited electrodes (closed) and by the solution for electrodes left open (open). Hence the different assumptions on the state of stress/strain are responsible for this behaviour. Therefore a comparison has to be performed with respect to the influence of electro-mechanical coupling. For that sake, ratios between the natural frequencies obtained by the coupled formulations and the purely elastic ones are plotted in Fig. 2. Fig. 2 shows an excellent agreement between analytic results and FE calculations. It is also interesting to note that the influence of different electric conditions is mostly important for the first natural frequency; it is not present for the even-numbered frequencies and tends to zero for the higher natural frequencies. The non-local formulation, requiring integration with respect to the span of the panel, explains this behaviour. Most important, this behaviour is also reflected by the FE calculations, resulting in the conclusion that it is necessary to use the non-local theory in order to obtain reasonable results for electrodes that are left open. Fig. 3 shows the mode shapes for the first two eigenmodes, for which normalization with respect to the cross-sectional rotation has been performed. For the first eigenmode, the mode shapes for deflection and cross-sectional rotation are different for different electric conditions, however quite similar to the elastic mode shapes. For the second mode, the

Table 1
Natural frequencies for the hinged–hinged panel (rad s^{-1})

	1st	2nd	3rd	4th	5th	6th
Elastic/FE	864.4	3276.0	6830.9	11,130	15,880	20,891
Elastic/analytic	840.1	3186.6	6650.6	10,844.5	15,481.8	20,376.8
Closed/FE	889.1	3375.5	7056.3	11,534	16,517	21,818
Closed/analytic	863.0	3279.3	6862.6	11,228.1	16,092.4	21,271.9
Open/FE	942.5	3375.5	7096.1	11,534	16,543	21,818
Open/analytic	912.0	3279.3	6900.1	11,228.1	16,118.2	21,271.9

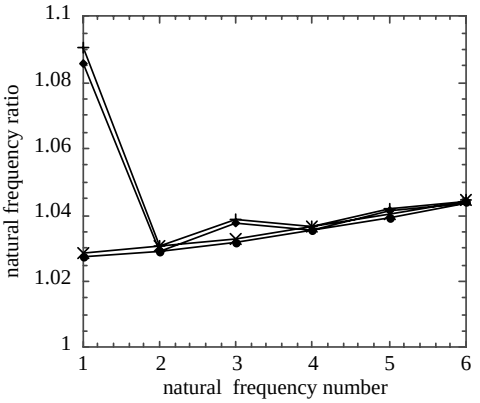

Fig. 2. Natural frequency ratio between electro-mechanically coupled natural frequencies and elastic natural frequencies for the hinged–hinged panel: —●— closed/analytic; —×— closed/FE; —◆— open/analytic; —|— open/FE.

mode shapes are nearly identical. It is also interesting to note the behaviour of the in-plane distribution of the electric potential χ in the vicinity of the edges, as depicted in Fig. 3c. This reflects the necessity of satisfying electric boundary conditions in the present theory. In Fig. 3c, an approximation for the in-plane distribution of the electric potential has additionally been plotted. This approximation is

$$\chi = -\frac{\hat{e}}{\hat{\eta}}\frac{\partial \psi}{\partial X}. \tag{35}$$

The approximation is quite good, except in the vicinity of the edges, which are located at $X = (0, L)$. This simplified plate theory can be found in Krommer and Irschik [20]. For more complicated vibration problems, for which approximate methods have to be used, the eigenmodes of the coupled problem can be approximated by the ones for the elastic problem, and by considering Eq. (35) for χ. For pointing out more clearly the difference between different electric conditions, Fig. 4 presents plots of the mode shapes for the electric potential distribution in the upper layer. Fig. 4a and b show the mode shapes for the first mode; for short-circuited electrodes, see Fig. 4a, and for electrodes left open, see Fig. 4b. The mode shape for the first mode is significantly different in the two cases. It can be also seen from Fig. 4b that the equipotential area condition at the electrodes is satisfied for electrodes left open, a requirement that motivated the non-local formulation developed in Section 2. For the second mode, the mode shapes are identical for short-circuited electrodes and for electrodes left open, see Fig. 4c.

Tables 2–4 present the results for the natural frequencies for other types of support conditions. The corresponding natural frequency ratios are plotted in Figs. 5–7. For the clamped–clamped panel, see Table 2 and Fig. 5, results for short-circuited electrodes and electrodes left open are identical. This is no surprise, because all boundary conditions are of the kinematic type. Thus the non-local terms do not influence the solution. For all types of support conditions, it is seen that the influence of electro-mechanical coupling increases with increasing natural frequency number. In contrast, the difference between the electric conditions at the electrodes decreases. This

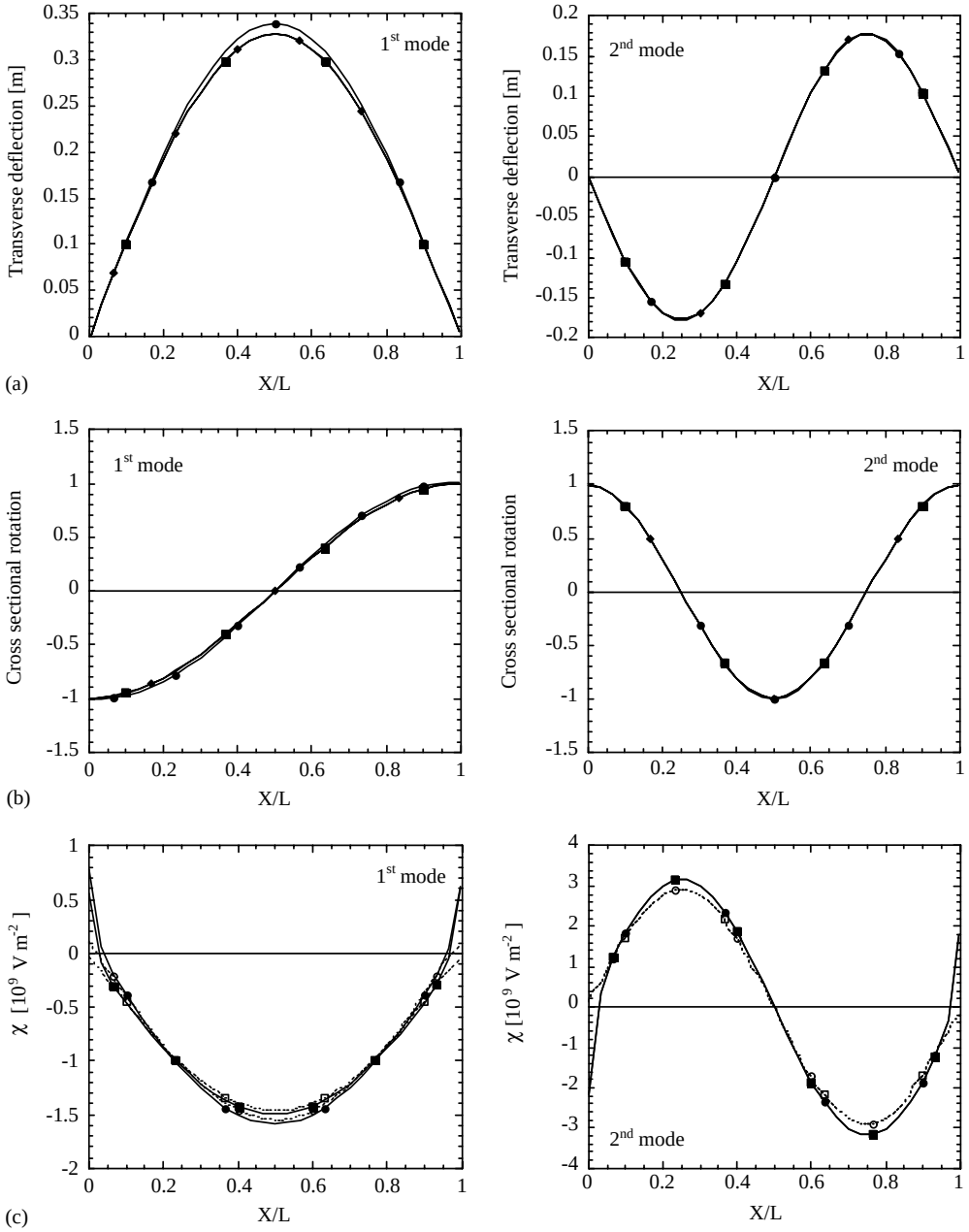

Fig. 3. First and second mode shapes for the hinged–hinged panel: (a) transverse deflection; (b) cross-sectional rotation; —●— open; —■— closed; —◆— elastic; (c) in-plane distribution of electric potential; —■— closed; - - -□- - - closed/approximated; —●— open; - - -○- - - open/approximated.

difference is mostly significant for the first natural frequency, especially for statically determinate panels. For redundant panels, the difference is not high, and it vanishes for the clamped–clamped panel.

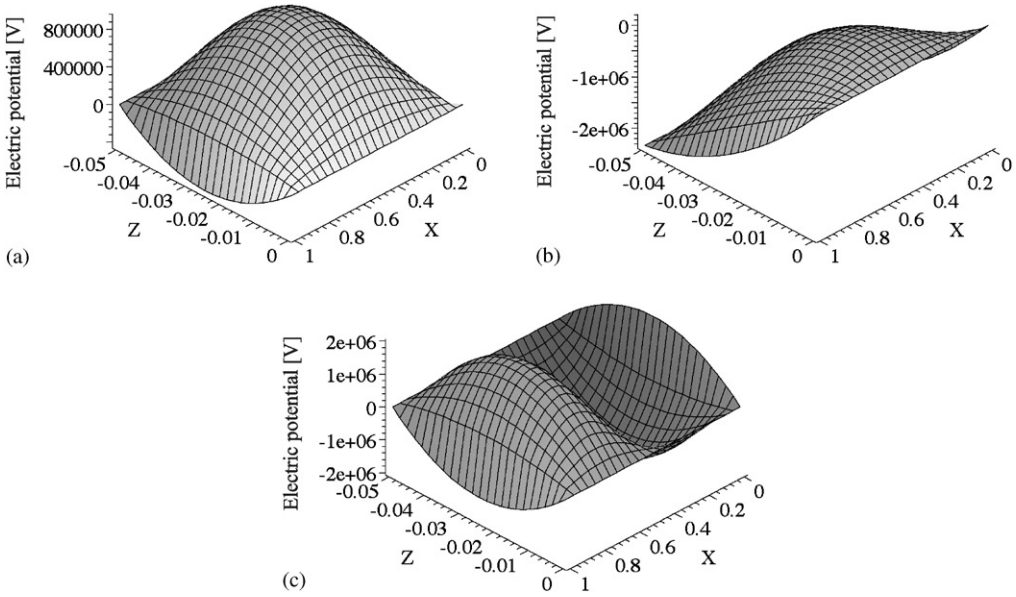

Fig. 4. Mode shapes of the electric potential for the hinged–hinged panel: (a) short-circuited electrodes—first mode; (b) electrodes left open—first mode; (c) short-circuited electrodes and electrodes left open-second mode.

Table 2
Natural frequencies for the clamped–clamped panel (rad s^{-1})

	1st	2nd	3rd	4th	5th	6th
Elastic/FE	1856.3	4688.1	8367.5	12,577	17,135	21,924
Elastic/analytic	1796.5	4551.5	8143.1	12,258.9	16,716.6	21,398.5
Closed/FE	1912.5	4844.1	8677.2	13,095	17,914	23,018
Closed/analytic	1849.3	4701.2	8444.0	12,766.2	17,484.3	22,479.5
Open/FE	1912.5	4844.1	8677.2	13,095	17,914	23,018
Open/analytic	1849.3	4701.2	8444.0	12,766.2	17,484.3	22,479.5

Table 3
Natural frequencies for the clamped–free panel (rad s^{-1})

	1st	2nd	3^{rd}	4th	5th	6th
Elastic/FE	312.4	1854.1	4822.5	8648.4	13,035	17,765
Elastic/analytic	302.3	1798.5	4687.6	8421.4	12,708.6	17,334.8
Closed/FE	321.16	1908.8	4975.0	8947.9	13,532	18,511
Closed/analytic	310.4	1849.6	4832.0	8707.1	13,188.8	18,060.4
Open/FE	335.4	1937.1	4998.6	8970.7	13,552	18,531
Open/analytic	323.8	1875.0	4854.4	8728.6	13,207.7	18,078.1

Table 4
Natural frequencies for the clamped–hinged panel (rad s^{-1})

	1st	2nd	3rd	4th	5th	6th
Elastic/FE	1318.0	3977.4	7610.9	11,871	16,523	21,420
Elastic/analytic	1277.8	3864.2	7407.5	11,568.3	16,114.7	20,899.7
Closed/FE	1356.7	4103.6	7877	12,331	17,231	22,430
Closed/analytic	1313.8	3983.5	7662.0	12,012.4	16,803.3	21,888.1
Open/FE	1371.3	4114.5	7886.9	12,338	17,238	22,435
Open/analytic	1326.9	3994.1	7671.0	12,019.8	16,809.5	21,893.2

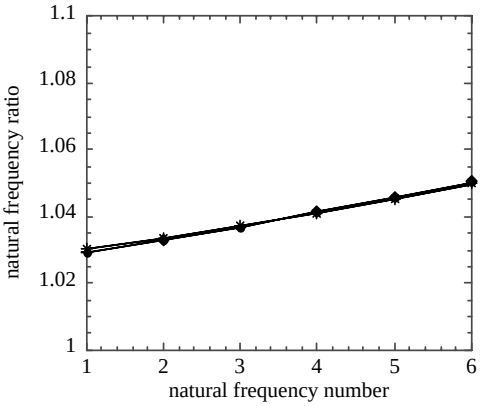

Fig. 5. Natural frequency ratio between electro-mechanically coupled natural frequencies and elastic natural frequencies for the clamped–clamped panel: —●— closed/analytic; —×— closed/FE; —◆— open/analytic; —|— open/FE.

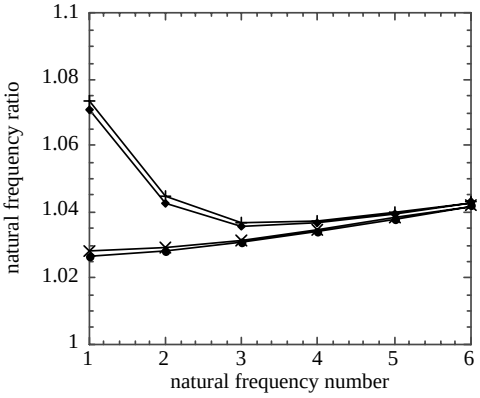

Fig. 6. Natural frequency ratio between electro-mechanically coupled natural frequencies and elastic natural frequencies for the clamped-free panel: —●— closed/analytic; —×— closed/FE; —◆— open/analytic; —|— open/FE.

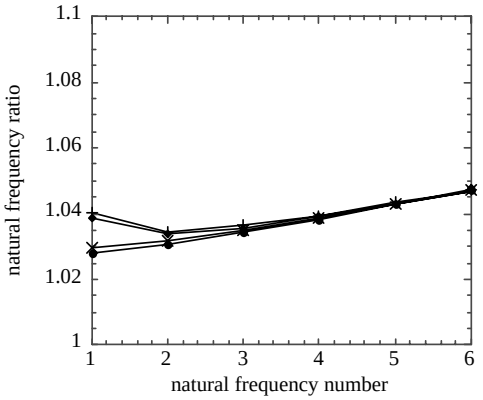

Fig. 7. Natural frequency ratio between electro-mechanically coupled natural frequencies and elastic natural frequencies for the clamped–hinged panel: —●— closed/analytic; —×— closed/FE; —◆— open/analytic; —|— open/FE.

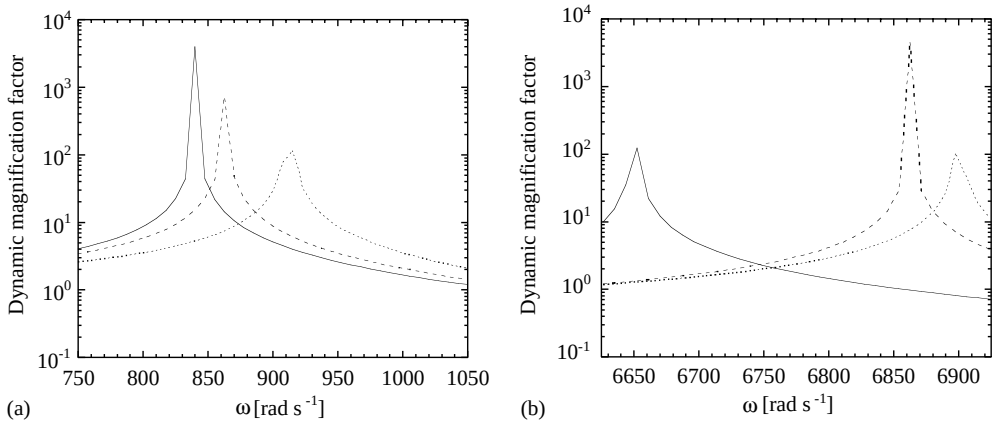

Fig. 8. Dynamic magnification factor for the hinged–hinged panel: (a) vicinity of the first natural frequency; (b) vicinity of the third natural frequency; —— decoupled; - - - - - - voltage; . . . . . charge.

3.1.2. Forced vibrations

A piezoelectric moment $m^{a,eff}$ of amount $80.82\,\mathrm{N\,m\,m^{-1}}$, which is produced by either applying an electric voltage $V^1 = -V^2 = 100\,\mathrm{V}$ or by applying a total charge $Q^1 = -Q^2 = 3.46 \times 10^{-5}\,\mathrm{C\,m^{-1}}$, acts on the panel. The dynamic magnification factor $|y(\omega)/y(\omega = 0)|$ of the sensor signal, see Eq. (21), is plotted in Figs. 8 and 9. Additional results obtained by utilizing a decoupled theory, which neglect the influence of the mechanical deformation on the electric field, are included in Figs. 8 and 9. In Fig. 8, the dynamic magnification factor for a hinged–hinged panel is presented in the vicinity of the first and the third natural frequencies. In the vicinity of the second natural frequencies, no peaks are shown by the dynamic magnification factor because the spanwise constant distribution of the actuation does not induce vibrations in the even numbered

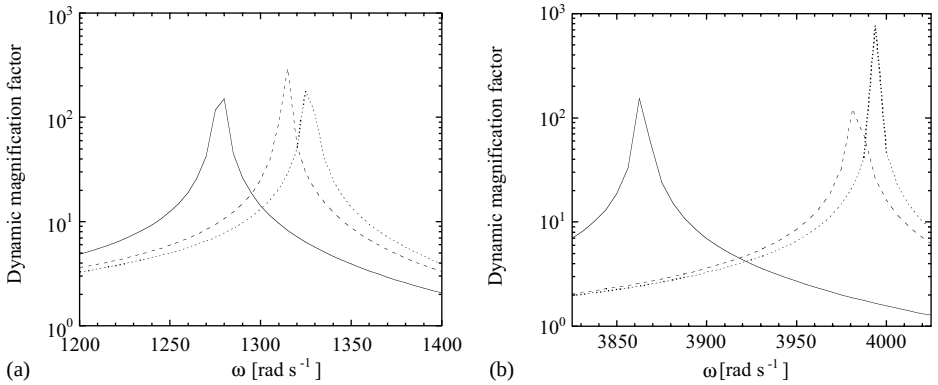

Fig. 9. Dynamic magnification factor for the clamped–hinged panel: (a) vicinity of the first natural frequency; (b) vicinity of the second natural frequency; —— decoupled; - - - - - - voltage; . . . . . charge.

modes, which are skew-symmetric. Also, the shifting of natural frequencies due to the electro-mechanical coupling is nicely reflected in Fig. 8. With increasing natural frequency number, this shifting becomes more important. This behaviour is in agreement with the one discussed in the previous section on natural frequencies. Fig. 9 finally shows the dynamic magnification factor for a clamped–hinged panel in the vicinity of the first and second natural frequencies. The behaviour is similar to the one for the hinged–hinged panel; nevertheless, vibrations in the second mode are actuated for the clamped–hinged support conditions. Note that the behaviour in the vicinity of the peaks in Figs. 8 and 9 is due to the discretization in the plots.

4. Conclusion

It was the main intention of this paper to incorporate the influence of electro-mechanical coupling by means of the direct piezoelectric effect and the converse piezoelectric effect upon the mechanical and electrical behaviour of Reissner–Mindlin-type composite plates. A theory has been presented, which can be said to represent a straightforward extension of the Reissner–Mindlin plate theory with respect to these requirements. Its formal structure is quite similar to the purely elastic theory and the purely electric theory. The mechanical field equations in terms of stress resultants and stress couples are identical to the equations valid in elasticity. The electrical field equations formulated in terms of resultants of the electric displacement vector are also identical to equations that can be used in electrostatics. Not taking into account the influence of mechanical fields upon the electric field would lead to the simple description of a capacitor. The coupled behaviour is included in the constitutive relations only. In these constitutive relations, the modelling of electroded piezoelectric layers with an unspecified electric potential difference is incorporated by means of non-local elastic terms. Finally, numerical examples have been presented, demonstrating the capability of the present theory to account for the electro-mechanically coupled dynamic behaviour.

Acknowledgements

Support of the author by the MAX-KADE foundation and the Austrian Academy of Sciences is gratefully acknowledged.

Appendix A. Nomenclature

For a material with the symmetry properties of a hexagonal system of class 6mm, e.g., PZT-5A, the linearized three-dimensional constitutive relations can be written in technical notations as

$$\begin{bmatrix} \sigma_{11} \\ \sigma_{22} \\ \sigma_{33} \\ \sigma_{23} \\ \sigma_{13} \\ \sigma_{12} \\ D_1 \\ D_2 \\ D_3 \end{bmatrix} = \begin{bmatrix} Q_{11} & Q_{12} & Q_{13} & 0 & 0 & 0 & 0 & 0 & -e_{31} \\ Q_{12} & Q_{11} & Q_{13} & 0 & 0 & 0 & 0 & 0 & -e_{31} \\ Q_{13} & Q_{13} & Q_{33} & 0 & 0 & 0 & 0 & 0 & -e_{33} \\ 0 & 0 & 0 & Q_{44} & 0 & 0 & 0 & -e_{15} & 0 \\ 0 & 0 & 0 & 0 & Q_{44} & 0 & -e_{15} & 0 & 0 \\ 0 & 0 & 0 & 0 & 0 & Q_{66} & 0 & 0 & 0 \\ 0 & 0 & 0 & 0 & e_{15} & 0 & \epsilon_{11} & 0 & 0 \\ 0 & 0 & 0 & e_{15} & 0 & 0 & 0 & \epsilon_{11} & 0 \\ e_{31} & e_{31} & e_{33} & 0 & 0 & 0 & 0 & 0 & \epsilon_{33} \end{bmatrix} \begin{bmatrix} \varepsilon_{11} \\ \varepsilon_{22} \\ \varepsilon_{33} \\ \gamma_{23} \\ \gamma_{13} \\ \gamma_{12} \\ E_1 \\ E_2 \\ E_3 \end{bmatrix},$$

$$Q_{66} = \frac{Q_{11} - Q_{12}}{2}.$$

The (1,2)-plane in such a material is an isotropic plane. For PZT-5A, the values of the material parameters are:

Elastic moduli: $[10^9 \times \mathrm{N\,m^{-2}}]$

$$Q_{11} = 121, \quad Q_{12} = 75.4, \quad Q_{13} = 75.2, \quad Q_{33} = 111, \quad Q_{44} = 21.8, \quad Q_{66} = 22.8.$$

Piezoelectric moduli: $[\mathrm{C\,m^{-2}}]$

$$e_{31} = -5.46, \quad e_{33} = 15.8, \quad e_{15} = 12.32.$$

Permittivities: $\epsilon_0 = 8.854 \times 10^{-12}\ \mathrm{As\,V^{-1}\,m^{-1}}$

$$\epsilon_{11} = 1730\epsilon_0, \quad \epsilon_{33} = 1700\epsilon_0.$$

Density: $[\mathrm{kg\,m^{-3}}]$

$$\rho = 7750.$$

The material parameters of Eq. (29) are calculated from the above as

$$Y = Q_{11} - \frac{Q_{13}Q_{13}}{Q_{33}}, \quad G = Q_{44}, \quad \bar{e} = e_{31} - \frac{e_{33}Q_{13}}{Q_{33}}, \quad \bar{h} = e_{15}, \quad \eta = \epsilon_{33} + \frac{e_{33}e_{33}}{Q_{33}}, \quad \epsilon = \epsilon_{11}.$$

References

[1] J. Tani, T. Takagi, J. Qiu, Intelligent material systems: application of functional materials, Applied Mechanics Review 51 (1998) 505–521.

[2] H.S. Tzou, Multifield transducers, devices, mechatronic systems and structronic systems with smart materials, The Shock and Vibration Digest 30 (1998) 282–294.

[3] S.S. Rao, M. Sunar, Piezoelectricity and its use in disturbance sensing and control of flexible structures: a survey, Applied Mechanics Review 47 (1994) 113–123.

[4] G. Kirchhoff, Über das Gleichgewicht und die Bewegung einer elastischen Scheibe, Zeitschrift für Reine und Angewandte Mathematik 40 (1850) 51–58.

[5] E. Reissner, On the theory of bending of elastic plates, Journal of Mathematics and Physics 23 (1944) 184–191.

[6] E. Reissner, The effect of transverse shear deformation on the bending of elastic plates, Journal of Applied Mechanics 12 (1945) A69–A77.

[7] H. Hencky, Über die Berücksichtigung der Schubverzerrung in ebenen Platten, Ingenieur-Archiv 16 (1947) 72–76.

[8] R.D. Mindlin, Influence of rotatory inertia and shear on flexural motions of isotropic plates, Journal of Applied Mechanics 18 (1951) 31–38.

[9] R.D. Mindlin, Higher frequency vibrations of crystal plates, Quarterly Applied Mathematics 19 (1961) 51–61.

[10] H.F. Tiersten, Linear Piezoelectric Plate Vibrations, Plenum Press, New York, 1969.

[11] C.-K. Lee, Theory of laminated piezoelectric plates for the design of distributed sensors/actuators. Part I: Governing equations and reciprocal relationships, Journal of the Acoustical Society of America 87 (3) (1990) 1144–1158.

[12] D.K. Miu, Mechatronics: Electromechanics and Contromechanics, Springer, New York, 1993.

[13] T.R. Tauchert, Piezothermoelastic behavior of a laminated plate, Journal of Thermal Stresses 15 (1992) 25–37.

[14] A. Benjeddou, M.A. Trinade, R. Ohayon, A unified beam finite element model for extension and shear piezoelectric actuation mechanisms, Journal of Intelligent Material Systems and Structures 8 (1997) 1012–1025.

[15] N.N. Rogacheva, The Theory of Piezoelectric Shells and Plates, CRC Press, Boca Raton, FL, 1994.

[16] H. Ling-Hui, Axisymmetric response of circular plates with piezoelectric layers: an exact solution, International Journal of Mechanical Sciences 40 (12) (1998) 1265–1279.

[17] M. Krommer, On the correction of the Bernoulli–Euler beam theory for smart piezoelectric beams, Smart Materials and Structures 10 (2001) 668–680.

[18] M. Krommer, A non-local formulation for the electromechanically coupled behavior of piezoelastic composite thin plates, Smart Materials and Structures (2002), submitted for publication.

[19] M. Krommer, H. Irschik, On the influence of the electric field on free transverse vibrations of smart beams, Smart Materials and Structures 8 (1999) 401–410.

[20] M. Krommer, H. Irschik, A Reissner–Mindlin-type plate theory including the direct piezoelectric and the pyroelectric effect, Acta Mechanica 141 (2001) 51–69.

[21] H.F. Tiersten, Equations for the extension and flexure of relatively thin electroelastic plates undergoing large electric field, in: J.S. Lee, G.A. Maugin, Y. Shindo (Eds.), Mechanics of Electromagnetic Materials and Structures, American Society of Mechanical Engineers, New York, AMD 161, MD 42, 1993, pp. 21–34.

[22] J.S. Yang, R.C. Batra, A theory of electroded thin thermopiezoelectric plates subject to large driving voltages, Journal of Applied Physics 76 (1994) 5411–5417.

[23] J.S. Yang, Equations for the extension and flexure of electroelastic plates under strong electric fields, International Journal of Solids and Structures 36 (1999) 3171–3192.

[24] A. Fernandes, J. Pouget, Accurate modelling of piezoelectric plates: single-layered plate, Archives of Applied Mechanics 71 (2001) 509–524.

[25] H.S. Tzou, R. Ye, Analysis of piezoelastic structures with laminated piezoelectric triangle shell elements, American Institute of Aeronautics and Astronautics Journal 34 (1) (1996) 110–115.

[26] H.-J. Lee, D.A. Saravanos, Generalized finite element formulation for smart multilayered thermal piezoelectric composite plates, International Journal of Solids and Structures 34 (26) (1997) 3355–3371.

[27] J.A. Mitchell, J.N. Reddy, A refined hybrid plate theory for composite laminates with piezoelectric laminae, International Journal of Solids and Structures 32 (16) (1995) 2345–2367.

[28] D.A. Saravanos, P.R. Heyliger, Mechanics and computational models for laminated piezoelectric beams, plates, and shells, Applied Mechanics Review 52 (10) (1999) 305–320.
[29] S.V. Gopinathan, V.V. Varadan, V.K. Varadan, Review and critique theories for piezoelectric laminates, Smart Materials and Structures 9 (1) (2000) 24–48.
[30] R. Suresh, G. Singh, G.V. Rao, An analytical solution for the flexural response of intelligent composite and sandwich panels, Acta Mechanica 152 (2001) 81–93.
[31] J. Bonet, R.D. Wood, Nonlinear Continuum Mechanics for Finite Element Analysis, Cambridge University Press, Cambridge, 1997.
[32] M. Krommer, H. Irschik, An electromechanically coupled theory for piezoelectric beams taking into account the charge equation of electrostatics, Acta Mechanica 154 (2002) 141–158.
[33] M. Krommer, An electromechanically coupled plate theory taking into account the influence of shear, rotatory inertia and electric field, Mechanics Research Communications 27 (2000) 197–202.
[34] W. Nowacki, Dynamic Problems of Thermoelasticity, Noordhoff, Leyden, 1975.
[35] H. Parkus, Variational Principles in Thermo- and Magneto-Elasticity, Springer, Vienna, New York, 1970.
[36] A.C. Eringen, G.A. Maugin, Electrodynamics of Continua I: Foundations and Solid Media, Springer, New York, 1990.
[37] J.N. Reddy, Mechanics of Laminated Composite Structures: Theory and Analysis, Wiley, New York, 1996.
[38] P. Heyliger, S. Brooks, Free vibration of piezoelectric laminates in cylindrical bending, International Journal of Solids and Structures 32 (20) (1995) 2945–2960.